

Measurements and modelling of I₂, IO, OIO, BrO and NO₃ in the mid-latitude marine boundary layer

A. Saiz-Lopez¹, J. A. Shillito², H. Coe², and J. M. C. Plane¹

¹School of Environmental Sciences, University of East Anglia, Norwich, UK

²School of Earth, Atmospheric & Environmental Sciences, University of Manchester, Manchester, UK

Received: 26 August 2005 – Published in Atmos. Chem. Phys. Discuss.: 10 October 2005

Revised: 6 March 2006 – Accepted: 6 March 2006 – Published: 11 May 2006

Abstract. Time series observations of molecular iodine (I₂), iodine oxides (IO, OIO), bromine oxide (BrO), and the nitrate radical (NO₃) in the mid-latitude coastal marine boundary layer (MBL) are reported. Measurements were made using a new long-path DOAS instrument during a summertime campaign at Mace Head on the west coast of Ireland. I₂ was detected using the $B^3\Pi(0_u^+) - X^1\Sigma_g^+$ electronic transition between 535 and 575 nm. The I₂ mixing ratio was found to vary from below the detection limit (~5 ppt) up to a nighttime maximum of 93 ppt. Along with I₂, observations of IO, OIO and NO₃ were also made during the night. Surprisingly, IO and OIO were detected at mixing ratios up to 2.5 and 10.8 ppt, respectively. A model is employed to show that the reaction between I₂ and NO₃ is the likely nighttime source of these radicals. The BrO mixing ratio varied from below the detection limit at night (~1 ppt) to a maximum of 6 ppt in the first hours after sunrise. A bromine chemistry model is used to simulate the diurnal behaviour of the BrO radical, demonstrating the importance of halogen recycling through sea-salt aerosol. In the same campaign a zenith sky DOAS was employed to determine the column density variation of NO₃ as a function of solar zenith angle (SZA) during sunrise, from which vertical profiles of NO₃ through the troposphere were obtained. On several occasions a positive gradient of NO₃ was observed over the first 2 km, possibly due to dimethyl sulphide (DMS) removing NO₃ at the ocean surface.

polar tropospheric (Barrie et al., 1988; Finlayson-Pitts et al., 1990; McConnell et al., 1992; Hausmann and Platt, 1994; Hönninger and Platt, 2002) ozone. However, halogen radicals could play a key role in a number of other important tropospheric processes, including NO_x (NO and NO₂) and HO_x (OH and HO₂) chemistry, the oxidation of a range of organic molecules, and in the formation of ultra-fine particles. These impacts are discussed in greater detail below. In the mid-latitude MBL, BrO has recently been detected both by multi-axis DOAS (Leser et al., 2003) and long-path DOAS (Saiz-Lopez et al., 2004a). The source of bromine is almost certainly the release of species such as Br₂, BrCl and IBr from sea-salt aerosol, following the uptake from the gas phase, and subsequent aqueous-phase reactions, of hypohalous acids (HOX, where X=Br, I) (Vogt et al., 1996). In semi-polluted areas with higher NO_x, the uptake of dinitrogen pentoxide (N₂O₅), formed at night by the recombination of the NO₃ with NO₂, also leads to the release of BrNO₂ (Behnke et al., 1994). These heterogeneous mechanisms are supported by the observation that the bromide ions in sea-salt aerosols are substantially depleted (Sander et al., 2003). Once released into the gas phase, these bromine-containing compounds will photolyse rapidly during the day, and the resulting Br atoms react rapidly with O₃ to form BrO. The radical competes effectively with OH in the oxidation of DMS (Toumi, 1994; Saiz-Lopez et al., 2004a; von Glasow and Crutzen, 2004). Recent measurements of IO and OIO (Alicke et al., 1999; Allan et al., 2000a, 2001; Saiz-Lopez and Plane, 2004) have confirmed the importance of iodine chemistry in the MBL. The source of atmospheric iodine is the evasion of biogenic iodocarbons such as CH₃I, CH₂I₂, CH₂IBr and CH₂ICl from both the open ocean and coastal areas (Carpenter et al., 1999). It has recently been shown that I₂ is probably the major source of atmospheric iodine in certain coastal locations (Saiz-Lopez and Plane, 2004). Some types of macro-algae (e.g. Laminaria) accumulate iodine compounds at concentrations substantially above those

1 Introduction

Interest in atmospheric halogen chemistry has grown enormously in the past three decades, originally because of its active role in the destruction of stratospheric (Molina and Rowland, 1974; Wofsy et al., 1975; Farman et al., 1985) and

Correspondence to: J. M. C. Plane
(j.m.c.plane@leeds.ac.uk)

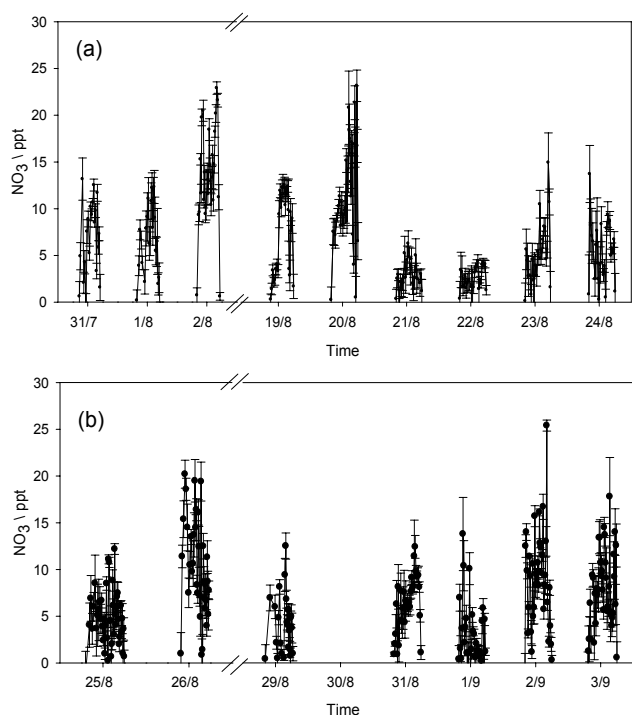


Fig. 1. NO_3 time series as measured by the LP-DOAS instrument during NAMBLEX. The mixing ratios are plotted together with the 2σ uncertainties.

in seawater, and this leads to direct injection of I_2 when the plants are exposed to the atmosphere at low tide (Truesdale et al., 1995; Kpper et al., 1998; McFiggans et al., 2004). A number of studies have proposed iodine as a significant catalyst in tropospheric O_3 depletion (Jenkin et al., 1985; Davis et al., 1996; Vogt et al., 1999; McFiggans et al., 2000). A recent study has also shown that the HO_2/OH ratio in the coastal MBL is significantly altered by IO (Bloss et al., 2005). Another potentially significant aspect of the iodine chemistry is the condensation of iodine oxide vapours, leading to the formation of new ultra-fine particles in the daytime marine atmosphere (O'Dowd et al., 2002; McFiggans et al., 2004; Saiz-Lopez et al., 2005). The role of I_2 in the production of new particles in coastal areas has been recently proposed by Saiz-Lopez and Plane (2004) and McFiggans et al. (2004), and explored in detail using an iodine chemistry model (Saiz-Lopez et al., 2005).

Field observations of the NO_3 radical over the past 25 years have demonstrated that it plays a major role in the chemistry of the nighttime troposphere (Platt et al., 1980, 1990; Heintz et al., 1996; Allan et al., 2000b, 2002a; Brown et al., 2003, 2004). Of particular interest is the reaction of NO_3 with DMS (Butkovskaya and LeBras, 1994). NO_3 also recombines with NO_2 to establish an equilibrium with N_2O_5 . The subsequent heterogeneous uptake of N_2O_5 on aqueous sea-salt aerosol both removes NO_x and activates halogens (see above).

In this paper we report results of the NAMBLEX (North Atlantic Marine Boundary Layer EXperiment) campaign which ran for 5 weeks in July/August 2002. Boundary layer observations of I_2 , IO, OIO, BrO and NO_3 were made by long-path differential optical absorption spectroscopy (DOAS), and measurements of the vertical concentration profiles of NO_3 by zenith sky DOAS. Note that although small subsets of the halogen data set have been published previously (Saiz-Lopez and Plane, 2004; Saiz-Lopez et al., 2004a), in this paper we present and discuss the complete data set. Box models are developed to investigate two particularly interesting features: the night-time chemistry of iodine, and the diurnal behaviour of BrO.

2 Experimental

2.1 Long-path DOAS instrument

The DOAS measurements were performed during NAMBLEX at the Mace Head Atmospheric Research Station on the west coast of Ireland ($53^\circ 20' \text{N}$, $9^\circ 54' \text{W}$). The long-path DOAS instrument was housed in an observatory on the foreshore at Mace Head. It consists of a Newtonian telescope containing the xenon arc lamp source, and the transmitting and receiving optics. The light beam was folded back to the transmitter by a retro-reflector situated 4.2 km away on Croaghnaekeela Island (see Fig. 2 in Saiz-Lopez et al., 2005), providing an optical absorption path of 8.4 km, about 5–20 m above sea level. Differential absorption spectra were collected by averaging for 30 min when measuring I_2 , IO, OIO and BrO, or 20 min when detecting NO_3 . More details on the instrument design and spectral deconvolution procedures are provided elsewhere (Plane and Saiz-Lopez, 2006). The following reference spectra were taken from the literature and adapted to the spectrometer instrument function: I_2 (Saiz-Lopez et al., 2004b), IO (Harwood et al., 1997), OIO (P. Spietz, University of Bremen, personal communication, 2005), BrO (Wahner et al., 1988) and NO_3 (Yokelson et al., 1994).

2.2 Zenith sky DOAS instrument

This instrument consists of a 0.8° field-of-view telescope, fixed in a zenith-viewing geometry and coupled to a spectrometer by means of a fibre optic cable. Spectra were recorded with a resolution of 0.5 nm in the $\lambda=640\text{--}700$ nm region for detection of NO_3 . A detailed description of the instrument is given in (Allan et al., 2002a). Spectra were acquired every 1–2 min (depending on scattered light levels) for approximately 2 h through sunrise ($87^\circ \leq \text{SZA} \leq 95^\circ$). The NO_3 column abundances were obtained using the same de-convolution method as for the long-path DOAS measurements, with a reference spectrum recorded after sunrise when the NO_3 mixing ratio is negligible due to the rapid photodissociation of the radical (Allan et al., 2002a). The vertical

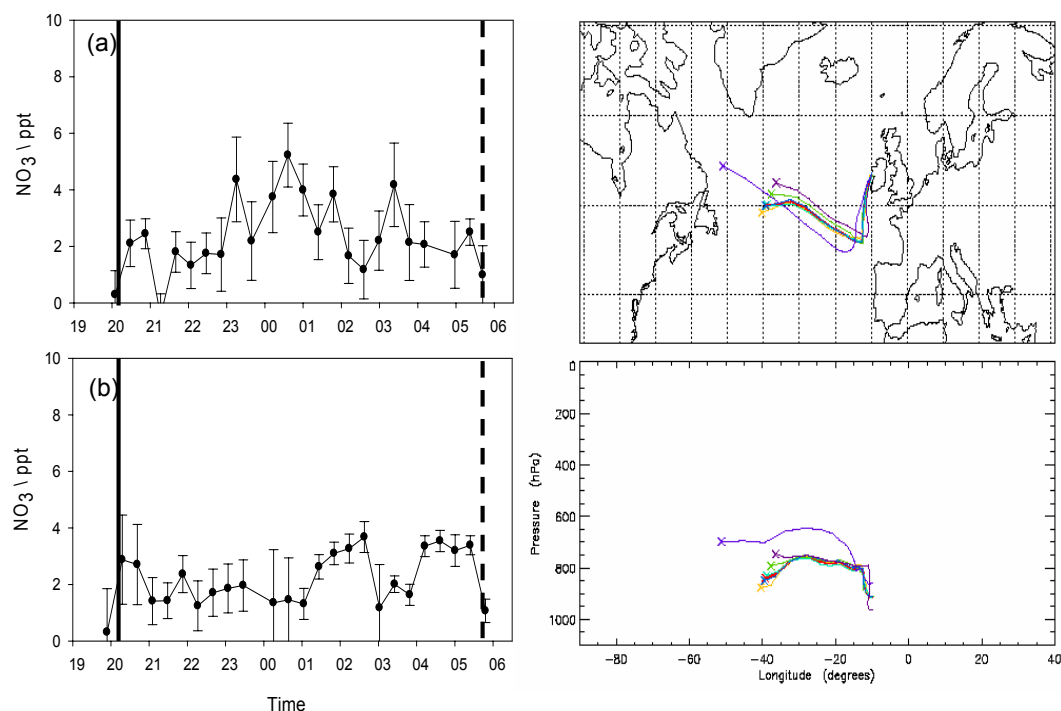


Fig. 2. NO_3 mixing ratios for a westerly air masses arrival day. The solid and broken black lines correspond to dusk and dawn times, respectively on 21 August (a) and 22 August (b). 5-day back trajectories for 21/22 August are shown in the right-hand panels. Each back trajectory shows the path of an air mass over a period of five days before its arrival at Mace Head. The arrival time is midnight and the colour coded trajectories correspond to different pressure levels.

concentration profile was then determined using an optimal estimation algorithm described below.

3 Results and discussion

3.1 Long-path DOAS measurements of NO_3

Observations of NO_3 were performed during 16 nights under different meteorological conditions. Figure 1 summarises the NO_3 time series set during the campaign. The maximum value reached during the observation period was 25 ppt, with averages of ~ 3 and 13 ppt for clean marine (westerly origin) and semi-polluted (easterly origin) air masses. These values are consistent with previously reported observations at the same location, under a similar range of meteorological conditions (Allan et al., 2000b). Comparable nighttime mixing ratio profiles have been reported in other marine areas (Heintz et al., 1996; Allan et al., 1999; Brown et al., 2004; Vrekoussis et al., 2004). The significant variations in NO_3 levels during the period of measurements can be explained by considering the back trajectories of the air masses arriving in the MBL at Mace Head. Figures 2 and 3 show two different types of air masses and the associated NO_3 mixing ratios. The solid and broken grey bars correspond to sunset and sunrise, respectively. Typically, NO_3 mixing ratios be-

low 5 ppt were associated with air masses from the Atlantic Ocean sector (Fig. 2a and b). By contrast, NO_3 mixing ratios above 10 ppt coincided with semi-polluted air masses from the UK or the European continent (Fig. 3a and b).

During NAMBLEX the broad-band cavity ring-down spectroscopy (BCCRDS) technique was also employed to make in-situ measurements of the NO_3 radical. An intercomparison of the local and long-path observations can be found in Bitter et al. (2006)¹. The in-situ BCCRDS values tended to be lower than those measured with the DOAS. This difference appears to be explained by titration of NO_3 by NO from soil emissions (Bitter et al., 2006¹). We have shown previously that under clean marine air conditions at Mace Head during summer, DMS controls the removal of NO_3 , whereas in semi-polluted air masses NO_3 removal is dominated by the indirect loss of N_2O_5 (Allan et al., 2000b).

A photochemical box model of the nighttime NO_3 chemistry (Allan et al., 2000b) was used to simulate the production of N_2O_5 from its equilibrium with NO_3 . The model was run under typical westerly clean marine conditions, for

¹Bitter, M., Ball, S. M., Povey, I. M., Jones, R. L., Saiz-Lopez, A., and Plane, J. M. C.: Measurements of NO_3 , N_2O_5 , OIO, I_2 , water vapour and aerosol optical depth by broadband cavity ringdown spectroscopy during the NAMBLEX campaign, Atmos. Chem. Phys. Discuss., in preparation, 2006.

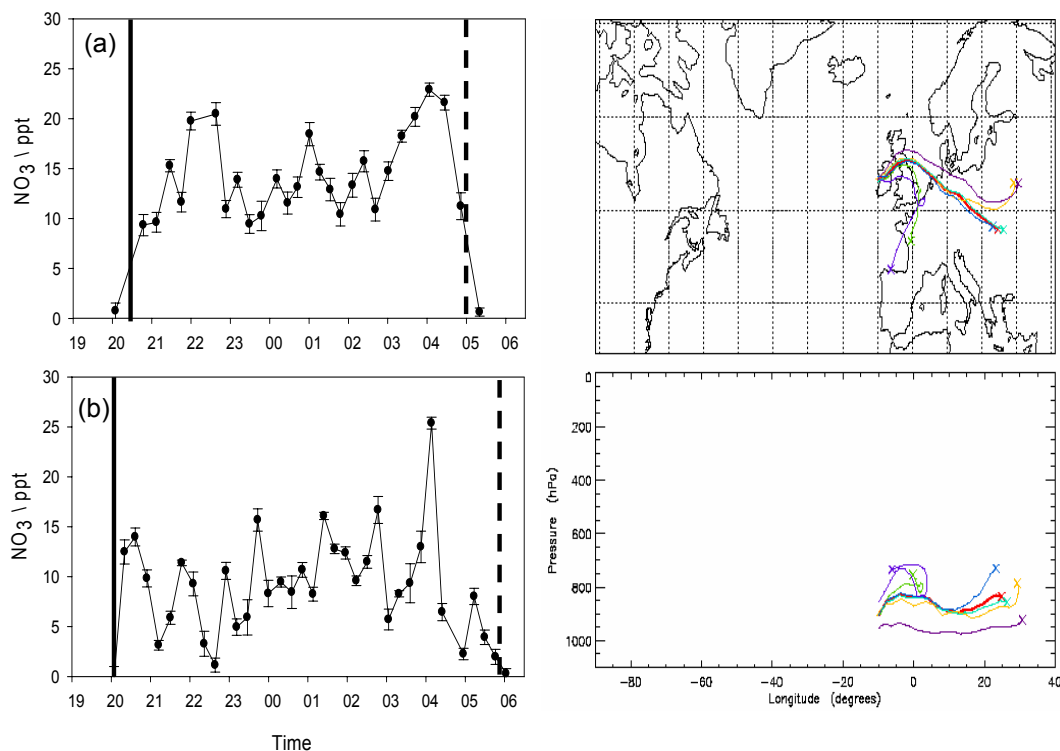


Fig. 3. Example of semi-polluted air masses and the NO_3 mixing ratio time-profiles for 1 August (a) and 3 September (b). The air mass back trajectories for 1 August are plotted on the right-hand.

which an average NO_3 mixing ratio of 3 ppt was observed. For marine air masses, the N_2O_5 accommodation coefficient in the model, $\gamma_{\text{N}_2\text{O}_5}$, was set at 0.03 (Behnke et al., 1997; Allan et al., 2000b). Under these clean marine conditions, with an aerosol volumetric surface area of $10^{-7} \text{ cm}^2 \text{ cm}^{-3}$ (Sander et al., 1999; von Glasow et al., 2002), the modelled N_2O_5 mixing ratio throughout the night is ~ 3 ppt. This N_2O_5 mixing ratio will be used in a bromine chemistry model (Sect. 3.6) to assess the contribution of NO_3 chemistry to halogen activation on sea-salt particles.

3.2 Zenith sky observations of NO_3 vertical profiles

NO_3 vertical column measurements were carried out at sunrise during six days, as shown in Fig. 4. The left-hand panels (Fig. 4a) show the expected dependence of NO_3 column on SZA: as the solar terminator sweeps down through the atmosphere, more and more of the overlying NO_3 is removed by photolysis. Note that the errors associated with individual column density measurements are quite variable. These uncertainties arise mostly from the visibility conditions and the temperature dependence of the NO_3 absorption cross-section (Allan et al., 2002a). The literature cross-section employed is that of Yokelson et al. (1994) at 280 K, a temperature which can be considered representative of the lower troposphere where the contribution to the NO_3 total absorption column

should be strongest. In Fig. 4a it can be seen that the NO_3 persisted after dawn on several occasions. This effect is most likely due to the thermal decomposition of N_2O_5 competing with photolysis to sustain the NO_3 mixing ratio past sunrise (Smith and Solomon, 1990; Smith et al., 1993; Allan et al., 2002a; Coe et al., 2002).

The conversion from column abundance to vertical mixing ratio profiles was made using the optimal estimation method (OEM) (Rodgers, 1976, 1990). Briefly, the forward model used is described by the expression $\mathbf{y}=\mathbf{K}\mathbf{x}$, where knowing the state of the system or weighing matrix function (\mathbf{K}) and the vertical mixing ratio profile (\mathbf{x}), the column density time series (\mathbf{y}) can be predicted. However, since \mathbf{x} is not known the forward model is inverted to give the backward model $\mathbf{x}=\mathbf{K}^{-1}\mathbf{y}$. The inversion process makes use of “a priori” information, i.e. the likely NO_3 vertical profile, to allow NO_3 vertical distribution information to be retrieved. \mathbf{K} comprises photolysis of NO_3 as a function of height, SZA and time (Coe et al., 2002).

In Fig. 4a the predicted column abundance (solid red line) using the forward model is compared with the measured, as a function of SZA. Figure 4b illustrates the corresponding retrieved NO_3 vertical concentration profiles. The vertical points are all independent pieces of information. The averaging kernel produced by the OEM method offers information on the vertical resolution possible from the zenith sky

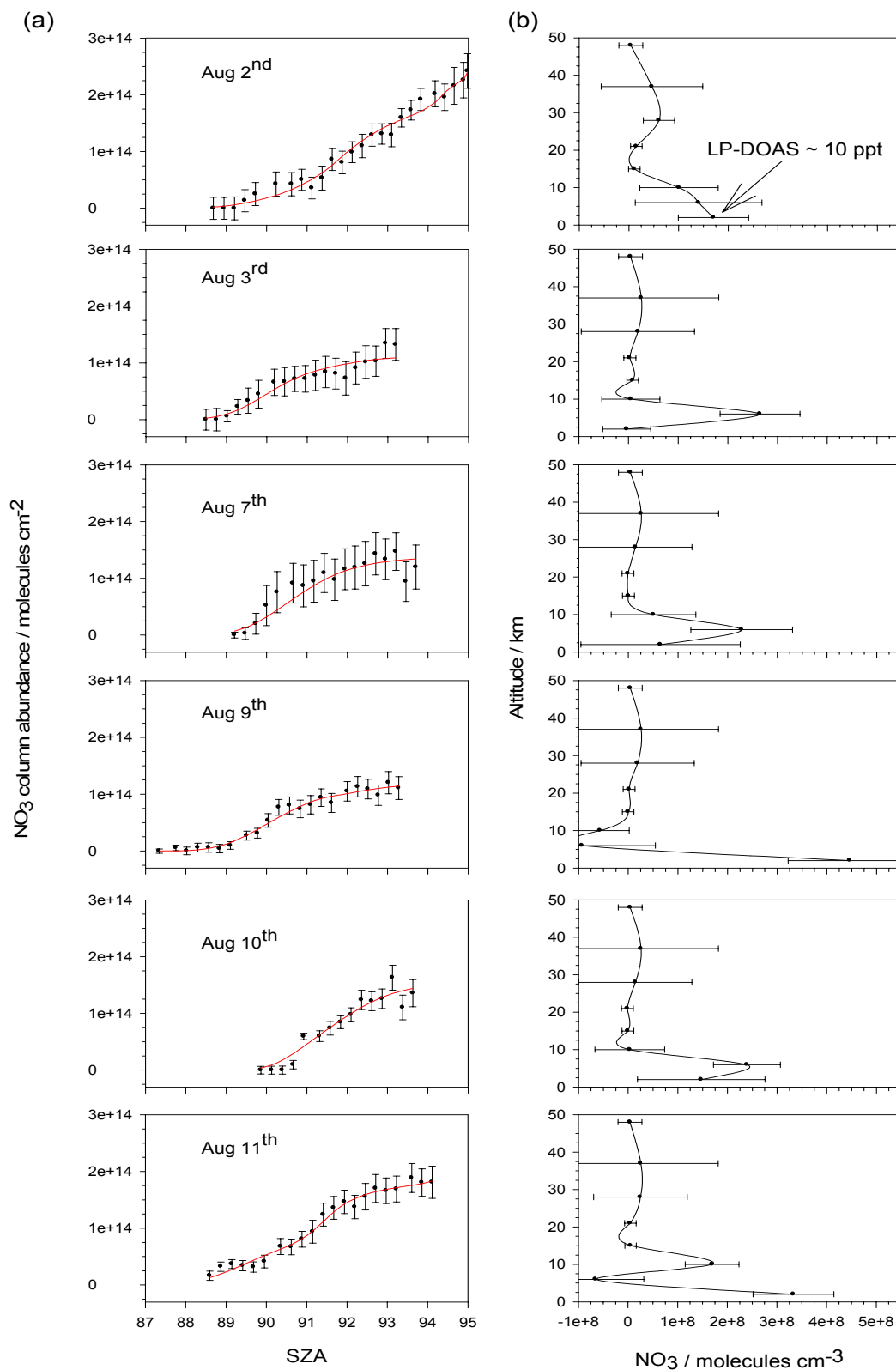


Fig. 4. (a) Zenith-sky spectroscopy measurements of the NO₃ column abundance as a function of SZA during six days of observations at Mace Head. The solid red line indicates the profile predicted by the OEM forward model. (b) The corresponding retrieved vertical concentration profile of NO₃.

absorption measurements; this was used to determine the retrieved altitudes as described in Coe et al. (2002). Figure 4b shows that at lower altitudes the vertical resolution is finer than that possible above 25 km (Coe et al., 2002). These profiles exhibit strong gradients, consistent with other observations (Aliwell and Jones, 1996; Allan et al., 2002a). On all six days, the highest NO_3 concentrations are in the mid- to low troposphere. There are probably three reasons for this. First, higher temperatures and NO_2 concentrations will cause NO_3 to be produced more rapidly from the oxidation of NO_2 by O_3 . Second, the thermal decomposition of N_2O_5 back to NO_3 will be faster. Third, DMS evading from the ocean will remove NO_3 at the base of the MBL, creating a positive gradient of NO_3 in the MBL. This may well explain the observations in clean marine conditions on 3, 7 and 10 August. During the NAMBLEX campaign, the vertical profile of DMS above Mace Head showed a marine influence up to an altitude of ~ 3 km due to local convective processes (Purvis et al., 2005). In addition to DMS, O_3 , NO_2 and sea-salt aerosol gradients may also have an impact on the vertical profile of NO_3 over Mace Head on these days. On the night of 2 August (when the site was influenced by semi-polluted continental air masses) long-path DOAS and zenith sky measurements of NO_3 were performed simultaneously. In Fig. 4b (top panel) the boundary layer measurement of ~ 10 ppt just before dawn is comparable to the 7 ppt or 1.8×10^8 molecule cm^{-3} retrieved for the lowest box in the vertical profile, which is centred at 2 km. Note that at the ground 2.5×10^8 molecule cm^{-3} is equivalent to 10 ppt, whereas at 5 km the mixing ratio is 20 ppt. This represents a factor of 5 increase over the lower layers on the nights of 2, 7 and 10 August. On 9 and 11 August, back trajectories show boundary layer air arriving after traversing north-south along the west coast of Ireland, which probably accounts for the relatively high NO_3 concentrations in the lowest box.

3.3 Iodine species (I_2 , IO, OIO)

Figures 5, 6 and 7 illustrate the time series of I_2 , IO and OIO during NAMBLEX respectively. The broken line in each of the panels shows the average DOAS detection limit for the particular species during the campaign. Measurements of I_2 were carried out on 18 days. As we have demonstrated in an accompanying paper (Saiz-Lopez et al., 2005), the photolysis lifetime of I_2 is so short (~ 15 s) that during daytime I_2 is very inhomogeneously distributed along the DOAS light path. Thus the daytime mixing ratios of I_2 (and IO) in Fig. 5 should be treated with caution – they are useful as relative rather than absolute measurements. The maximum I_2 mixing ratio observed during the campaign was 93 ppt. This was observed at night, when the average I_2 mixing ratio was considerably higher, as expected in the absence of photolysis.

Figure 5 shows that the I_2 mixing ratio is characterised by sharp peaks lasting for 30 to 45 min. Note that since the time resolution of the instrument is 30 min for the I_2 measure-

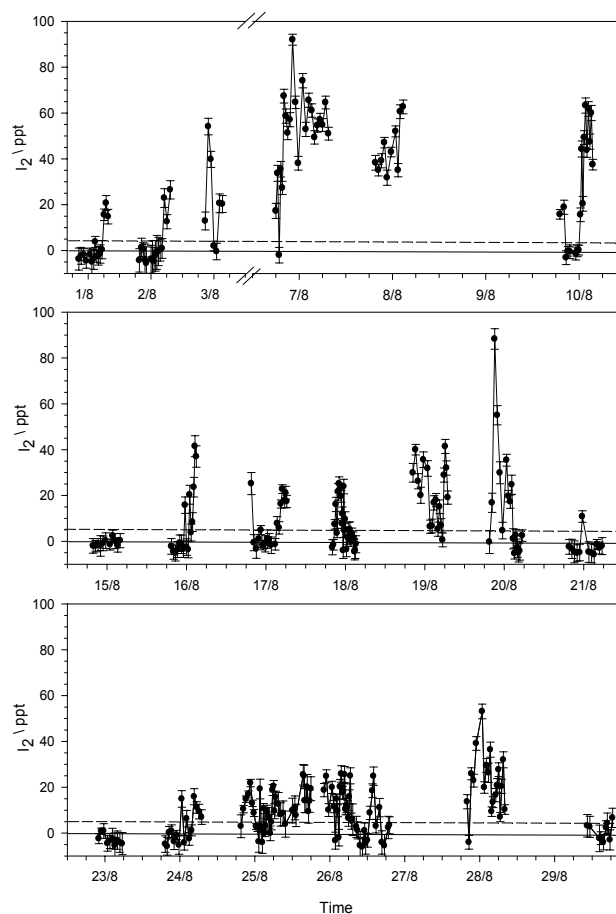


Fig. 5. Time series of I_2 at Mace Head during NAMBLEX. The mixing ratios are plotted with their 2σ uncertainties as well as their average detection limit through the campaign (horizontal broken line).

ments, I_2 could actually have been present in shorter peaks of higher concentration. These peaks always coincided with low tide. Indeed, a simple plot of I_2 mixing ratio versus tidal height exhibits a clear anti-correlation, as shown in Fig. 8. In contrast to the state of the tide, the I_2 mixing ratio did not correlate significantly with local wind direction. This is not surprising since the prevailing wind directions tended to be westerly or easterly, and macroalgae were exposed at both ends of the light path (see the map in Saiz-Lopez et al., 2005). Nevertheless, one potentially interesting detail is that I_2 was observed at low mixing ratios (~ 10 – 20 ppt) at night in westerly winds, irrespective of the state of the tide. This may indicate that I_2 is also produced over the open ocean, as originally proposed by Garland and Curtis (1981). Of course, other possible explanations are the re-circulation of air-masses that originated at the coast during low tide, or perhaps that moderate I_2 emissions still occur at higher states of the tide.

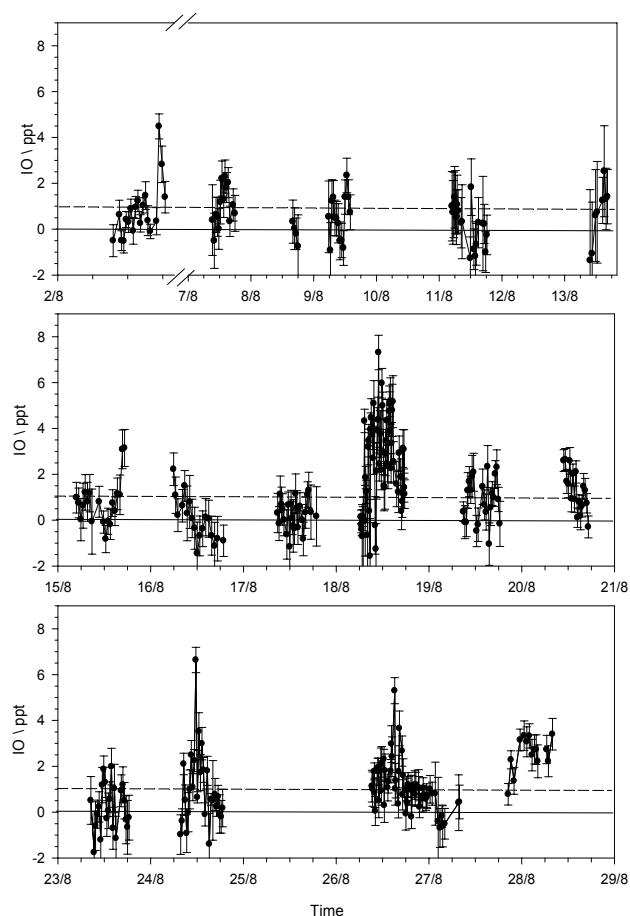


Fig. 6. Time series of IO at Mace Head during NAMBLEX.

Figure 6 shows the complete time series of IO during NAMBLEX, totalling 15 days of measurements. The maximum IO mixing ratio during the campaign was ~ 7 ppt, measured during daytime. This is in accord with previously reported IO observations at Mace Head (Alicke et al., 1999; Allan et al., 2000a). Note that this mixing ratio is probably the average of a rather inhomogeneous distribution along the DOAS path (Saiz-Lopez et al., 2005). During daytime, IO exhibited a clear anti-correlation with tidal height and solar irradiation, as shown in the mesh plot in Fig. 9. This is good evidence for its photochemical production from coastal emissions of I_2 (Saiz-Lopez and Plane, 2004). IO was only measured during two nights of NAMBLEX, when mixing ratios up to ~ 2.5 ppt were observed.

OIO measurements were made simultaneously with I_2 in the 535–575 nm wavelength region. During the day, OIO was not observed above the daytime detection limit of ~ 4 ppt (Fig. 7). The radical was only observed at night, with a maximum mixing ratio of 10.8 ppt. In fact, on this occasion the OIO peaked after local midnight, and about 2 h after a nighttime peak of I_2 at low tide. The observation that OIO is only detectable at night is consistent with previous measurements

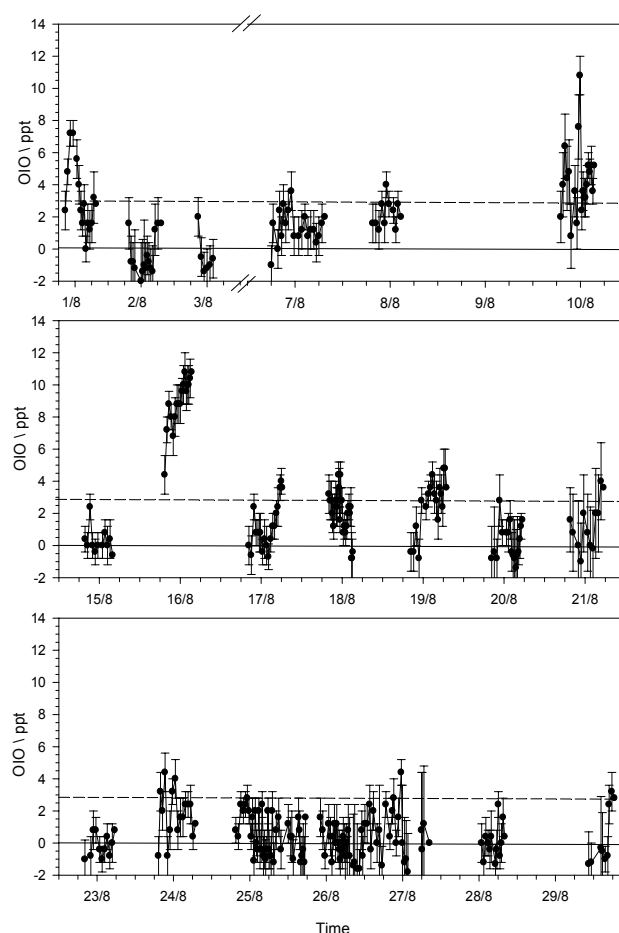


Fig. 7. Time series of OIO at Mace Head during NAMBLEX.

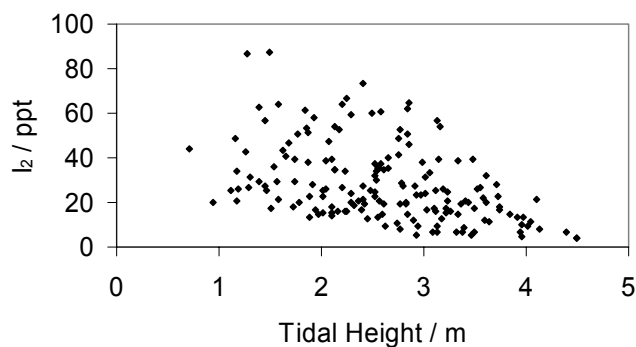


Fig. 8. Plot of I_2 mixing ratio versus tidal height at Mace Head.

made by us at Cape Grim (Tasmania), another remote marine location (Allan et al., 2001).

There appear to be two possible explanations for the absence of OIO during daytime. First, it could photolyse following absorption in the strong bands between about 470 and 610 nm. Whilst certain experimental evidence led us to conclude this was the case (Ashworth et al., 2002), we

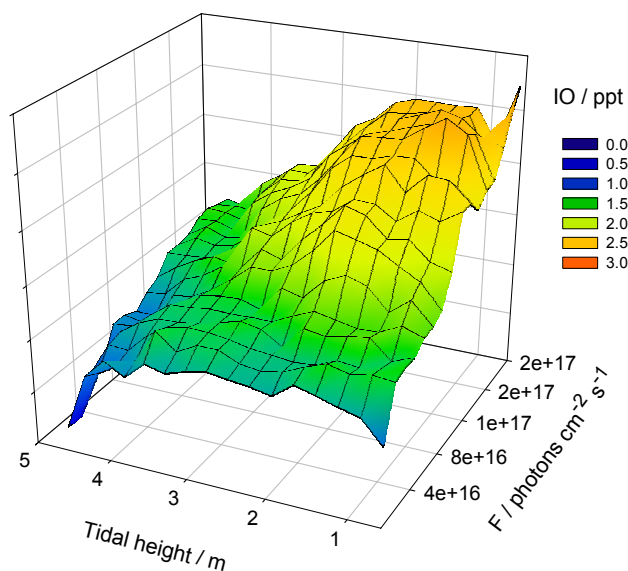


Fig. 9. Mesh plot showing the observed daytime IO as a function of tidal height and solar irradiance.

have recently shown that absorption leads to interconversion into the highly vibrationally-excited ground state rather than dissociation to $I+O_2$, so the quantum yield for photolysis is probably much less than 10% at 562 nm (Joseph et al., 2005). This is in agreement with a previous report from Ingham et al. (2000) that the yield of I was less than 5%. Nevertheless, a small probability of photolysis, integrated over the absorption bands, could still account for the removal of OIO during daytime (Saiz-Lopez et al., 2005). A second possibility is that OIO is removed during daytime by reaction with radicals that have marked diurnal cycles with daytime maxima, such as OH, NO and IO. Based on our current experimental and theoretical work (Plane et al., 2006), we believe that the most likely of these is IO, as discussed in our recent modelling study (Saiz-Lopez et al., 2005).

3.4 Nighttime iodine chemistry

In order to understand the source of IO and OIO during the night in the MBL, we have modified our existing iodine chemistry model (McFiggans et al., 2000; Saiz-Lopez et al., 2005). A plausible mechanism for the formation of atomic iodine at night is the reaction of $I_2+NO_3 \rightarrow INO_3+I$ (Chambers et al., 1992). The fate of INO_3 is probably either uptake on aerosol, or thermal dissociation. Assuming an accommodation coefficient, γINO_3 , of 0.05 and a clean MBL aerosol volumetric surface area of $10^{-7} \text{ cm}^2 \text{ cm}^{-3}$, the loss rate due to uptake on aerosols is $\sim 2.3 \times 10^{-5} \text{ s}^{-1}$. An upper limit to the rate of thermal dissociation of INO_3 at 285 K has been determined to be $4.5 \times 10^{-4} \text{ s}^{-1}$ (Allan and Plane, 2002b). Hence, at night in the MBL there is probably a competition between these processes.

We also consider in the model the thermal stabilities of I_2O_2 and I_2O_4 , dimers that form from the self reactions of IO and OIO, respectively. *Ab initio* quantum calculations, using a level of theory described previously (Allan and Plane, 2002b), show that the binding energy of the OIO dimer is only 72 kJ mol^{-1} , while that of the IO dimer (in the form IOIO) is about 86 kJ mol^{-1} . Using these binding energies, vibrational frequencies and rotational constants as input for a Rice-Ramsberger-Kassel-Markus (RRKM) calculation, we predict that the rates of dissociation of these dimer molecules will be fast at a typical mid-latitude MBL nighttime temperature of 285 K and a pressure of 1 atmosphere. I_2O_4 will dissociate back to OIO + OIO at a rate of $\sim 7 \times 10^3 \text{ s}^{-1}$. IOIO will dissociate to OIO+I and IO+IO at rates of ~ 12 and 4 s^{-1} , respectively. The atmospheric implication of these results will be a delay in the rate of disappearance of IO and OIO in the nighttime MBL. These dissociation rates, and the rate constant for the association of the OIO dimer (predicted from RRKM theory to be $\sim 5 \times 10^{-11} \text{ cm}^3 \text{ molecule}^{-1} \text{ s}^{-1}$ at 1 atm and 285 K), are included in the model.

In the model we prescribe the I_2 emission rate to have a Gaussian distribution, peaking at low tide with a standard half width of 22 min (Saiz-Lopez et al., 2005). The peak rate is adjusted to produce a peak I_2 mixing ratio of ~ 40 ppt, the average night-time I_2 peak that was observed during nocturnal low tide. The NO_3 mixing ratio was fixed at 10 ppt. Figure 10a shows the time-profiles of I_2 , IO and OIO. The O_3 mixing ratio is also shown, although the predicted O_3 loss rate is negligible ($3 \times 10^{-2} \text{ ppb h}^{-1}$). In the absence of photolysis, the I_2 mixing ratio decays much more slowly after low tide than during the day.

In this model run the IO and OIO mixing ratios peak at 2 ppt and 1.7 ppt, respectively, coincident with low tide. Hence, there are two things that differ from the nighttime observations. First, the OIO/IO ratio predicted by the model is 0.9, whereas the measurements indicate that this ratio is ~ 4 . Second, the observations show that the OIO peak occurs after I_2 reaches its maximum at low tide. Therefore, to reconcile the measurements with the model results, another route for converting IO to OIO, in addition to the self reaction of IO, is required. Although the reaction $IO+O_3 \rightarrow OIO+O_2$ is exothermic by about 150 kJ mol^{-1} (Misra and Marshall, 1998), a very small upper limit to the rate constant of $10^{-15} \text{ cm}^3 \text{ molecule}^{-1} \text{ s}^{-1}$ has been determined (Atkinson et al., 2000), so that this reaction would be too slow. Another candidate is the reaction:



Although this reaction does not appear to have been studied, it is also exothermic (by about 50 kJ mol^{-1}), and NO_3 is in general a more aggressive reactant than O_3 : for instance, it reacts about 10^5 times faster with I_2 .

When (1) is included in the model, the rate constant needs to be larger than $7 \times 10^{-12} \text{ cm}^3 \text{ molecule}^{-1} \text{ s}^{-1}$ in order to increase the modelled OIO/IO ratio to the observed ratio of

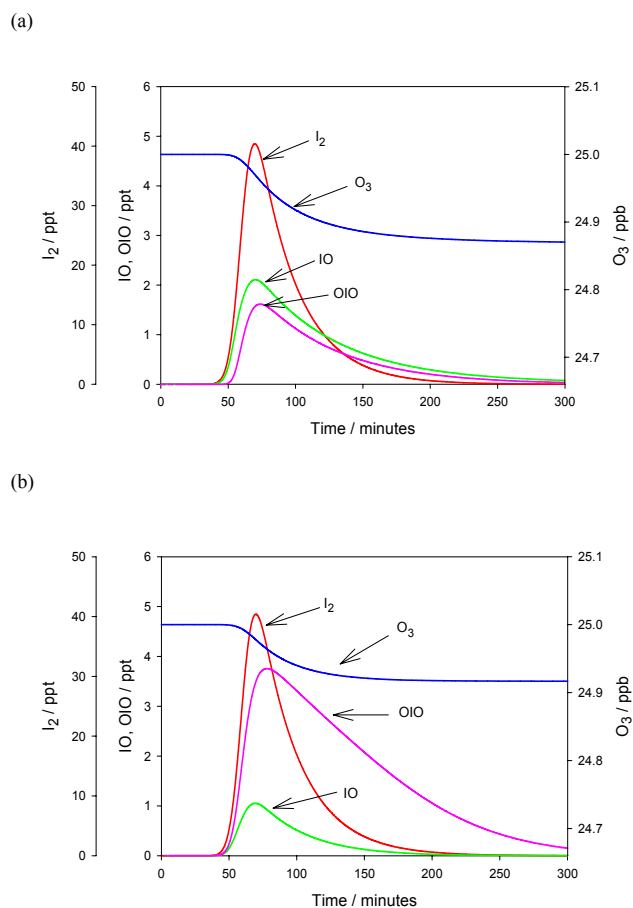


Fig. 10. (a) Nighttime run of the iodine model, with low tide 60 min after the start. (b) Model run with the same initial conditions as (a) but including the reaction $\text{IO} + \text{NO}_3 \rightarrow \text{OIO} + \text{NO}_2$.

4. This model run is shown in Fig. 10b; note that the OIO peak now occurs ~ 10 min after the maxima of I₂ and IO, as observed. In the observations, the delay between the OIO and I₂ peaks appeared to vary from a few minutes up to an hour; however, because of the 30 min time-resolution of the DOAS, this delay cannot be measured precisely. Although the model does not include vertical mixing or take account of inhomogeneity along the DOAS light path when comparing with the observations, it does include the uptake of OIO (and IO) onto a background aerosol loading typical of Mace Head (Coe et al., 2005). We therefore consider the level of agreement with the observations to be encouraging. A study of reaction (1) appears to be a priority to develop further understanding of night-time iodine chemistry.

3.5 BrO observations

BrO was measured over six days during NAMBLEX. A maximum mixing ratio of 6.0 ppt was observed, coinciding with westerly and relatively high speed winds (up to 11 m s^{-1}), whereas a mean daytime mixing ratio of 2.3 ppt was ob-

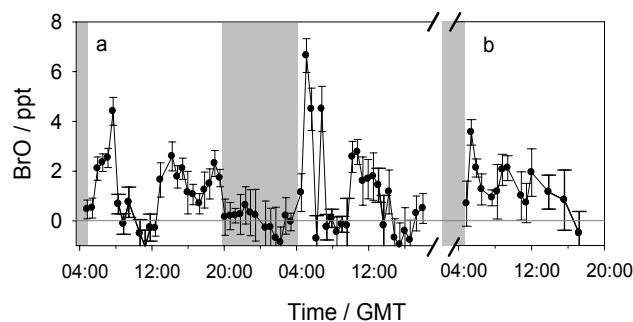


Fig. 11. Mixing ratio time-profile of BrO during three days of NAMBLEX measurements (3, 4 and 10 August).

served. The diurnal profile was characterised by a short-lived pulse after dawn. Figure 11 shows the mixing ratio time-profile during three days of observations (3, 4 and 10 August) when BrO was observed from dawn onwards. Sunrise occurred around 04:50 UT, with a 43 min twilight period defined as the interval when the SZA is between 96° and 90° . Twilight needs to be considered because, as we show below, some bromine atom precursors are very photolabile. After the BrO pulse, a rapid decrease in its mixing ratio was observed, followed by a partial recovery before noon. Figure 9 indicates that a second small maximum may also be present in the late afternoon before sunset, after which BrO decreased below the detection limit of the DOAS instrument (~ 1 ppt).

It is unlikely that the post-dawn BrO pulse results from the photolysis of organic bromine species, because of their long photolytic lifetimes in the lower atmosphere (Carpenter et al., 1999). One relatively short-lived alkyl bromide is CH_2IBr ; however, its photolytic lifetime is still about 1 h, and its mixing ratio in the MBL at Mace Head during summer is ~ 0.1 ppt (Carpenter et al., 1999). In any case, halocarbon emissions at Mace Head are driven by tidal height (Carpenter et al., 1999), and there is no correlation with tidal height evident in the BrO measurements.

Hence, the most likely BrO precursors are inorganic bromine species such as Br_2 , IBr , BrCl and BrNO_2 , which have built up after heterogeneous processing through sea-salt aerosol during the preceding night. At sunrise they are rapidly photolysed to yield Br atoms which react with O_3 to form BrO. An interesting problem is to determine which of these potential precursors is the main contributor to the post-sunrise BrO pulse. In Fig. 12a the absorption cross-sections of these four bromine precursors are plotted against wavelength, using data from Atkinson et al. (2000). It can be seen that IBr has the largest cross-section, peaking around 500 nm and extending throughout the visible region of the spectrum. IBr will therefore photolyse most readily around dawn. In contrast, BrNO_2 has an absorption cross-section nearly an order of magnitude smaller, peaking at 300 nm. The rates of photodissociation (J) of BrNO_2 , Br_2 , IBr and BrCl are

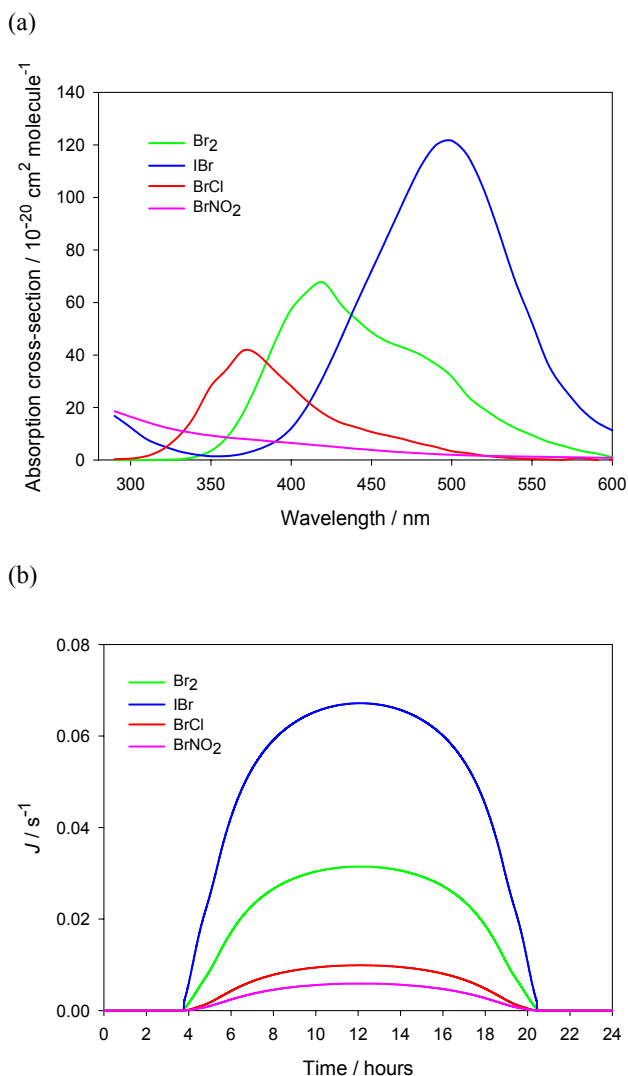
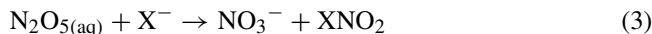


Fig. 12. (a) Absorption cross-sections of Br_2 , BrCl , IBr and BrNO_2 as a function of wavelength. (b) Diurnal variation of the corresponding rates of photolysis, calculated assuming a quantum yield of unity for clear sky conditions at Mace Head in August.

shown in Fig. 12b as a function of time of day, for the location of Mace Head in early August. The J values are calculated, assuming a quantum yield of unity, by an explicit two-stream radiation code (Thompson, 1984), where the incident actinic flux (photons $\text{cm}^{-2} \text{ s}^{-1} \text{ nm}^{-1}$) at the Earth's surface is obtained after attenuation through 50 atmospheric layers of 1 km height. Immediately after sunrise, J_{IBr} is twice as fast as J_{Br_2} and up to an order of magnitude faster than J_{BrNO_2} . Indeed, if BrNO_2 (and to a lesser extent BrCl) were the major sources of atomic Br, then the BrO pulse would be delayed in appearance and also less sharp.

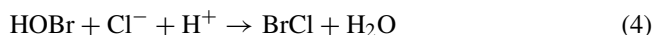
Laboratory studies of the uptake of N_2O_5 on a saline surface mimicking sea-salt aerosols, which are ~ 660 times more concentrated in Cl^- than Br^- , have been reported by

Behnke et al. (1994). The sequence of reactions is:



where X is Cl or Br. The authors found that $\sim 10\%$ of the released product was BrNO_2 , with 73% ClNO_2 and 17% Br_2 . Assuming this product yield for BrNO_2 and using the NO_3 chemistry model described in Sect. 3.1, we calculate that for clean marine conditions ($[\text{NO}_3]$ and $[\text{N}_2\text{O}_5] \sim 3$ ppt) the cycling through sea-salt aerosol during the night would yield a BrNO_2 mixing ratio of ≤ 0.2 ppt before sunrise.

When photolysis ceases after sunset, the uptake of HOBr or BrNO_3 on sea-salt aerosol will be their major removal pathways. These species will be rapidly recycled through heterogeneous reactions to gas-phase Br_2 and BrCl , depending on the availability of Cl^- and Br^- (Finlayson-Pitts, 2003):



If the Br^- concentration is sufficient (i.e., in freshly generated sea-salt aerosol), BrCl will be converted into Br_2 via Reactions (5) and (6). In aged sea-salt aerosol that is depleted in Br^- , BrCl becomes the major product (Fickert et al., 1999; Liu and Margerum, 2001; Adams et al., 2002).

Although the I^- content in sea-salt is negligible compared to Cl^- and Br^- , a similar mechanism to Reaction (4) can proceed following uptake of species such as HOI and INO_3 , leading to the release of ICl and IBr to the gas phase (Vogt et al., 1999; McFiggans et al., 2000). From laboratory experiments, the main di-halogen gas-phase product is IBr from freshly generated NaCl/NaBr surfaces with sufficient Br^- content. Release of ICl was only observed after depletion of Br^- (Holmes et al., 2001). The corresponding Henry's law constants ($\text{mol l}^{-1} \text{ atm}^{-1}$) for the different species are: $k_H(\text{BrNO}_2)=0.3$, $k_H(\text{Br}_2)=1.8$, $k_H(\text{BrCl})=0.59$ (Frenzel et al., 1998), $k_H(\text{ICl})=110$ and $k_H(\text{IBr})=24$ (Wagman et al., 1982).

Considering the above photodissociation rates and the mechanisms for recycling halogens through sea salt, it seems that Br_2 and IBr should be the primary sources of the large post-sunrise BrO pulses observed at Mace Head. However, from our DOAS observations there is no evidence of a post-sunrise pulse of IO (apart from when low tide coincides with sunrise). Putting this together with the fact that the solubility constant of IBr is an order of magnitude greater than that of Br_2 , we infer that Br_2 is probably the dominant source of Br at sunrise in this location.

Table 1. Bromine chemistry scheme used in the photochemical box model^a.

No	Reaction	Rate constant	Remarks ^b
(R1)	$\text{Br} + \text{O}_3 \rightarrow \text{BrO} + \text{O}_2$	$1.7 \times 10^{-11} e^{(-800/T)}$	1
(R2)	$\text{HBr} + \text{OH} \rightarrow \text{Br} + \text{H}_2\text{O}$	1.1×10^{-11}	1
(R3)	$\text{Br} + \text{HO}_2 \rightarrow \text{HBr} + \text{O}_2$	$1.5 \times 10^{-11} e^{(-600/T)}$	1
(R4)	$\text{Br} + \text{HCHO} \rightarrow \text{HBr} + \text{HCO}$	$7.7 \times 10^{-12} e^{(-580/T)}$	1
(R5)	$\text{Br} + \text{CH}_3\text{CHO} \rightarrow \text{HBr} + \text{CH}_3\text{CO}$	$1.8 \times 10^{-11} e^{(-460/T)}$	
(R6)	$\text{Br} + \text{NO}_2 + \text{M} \rightarrow \text{BrNO}_2$	$k_o = 4.2 \times 10^{-31} \times (\text{T}/300)^{-2.4}$ $k_\infty = 2.7 \times 10^{-11} \times (\text{T}/300)^{-0.0}$	1
(R7)	$\text{BrO} + \text{NO}_2 + \text{M} \rightarrow \text{BrNO}_3$	$k_o = 5.2 \times 10^{-31} \times (\text{T}/300)^{-3.2}$ $k_\infty = 6.9 \times 10^{-12} \times (\text{T}/300)^{-2.9}$	1
(R8)	$\text{BrO} + \text{HO}_2 \rightarrow \text{HOBr} + \text{O}_2$	$3.4 \times 10^{-12} e^{(540/T)}$	1
(R9)	$\text{BrO} + \text{NO} \rightarrow \text{Br} + \text{NO}_2$	$8.8 \times 10^{-12} e^{(260/T)}$	1
(R10)	$\text{BrO} + \text{CH}_3\text{SCH}_3 \rightarrow \text{CH}_3\text{SOCH}_3 + \text{Br}$	$1.5 \times 10^{-14} e^{(850/T)}$	1
(R11)	$\text{BrO} + \text{BrO} \rightarrow 2\text{Br} + \text{O}_2$	$2.4 \times 10^{-12} e^{(40/T)}$	1
(R12)	$\text{BrO} + \text{BrO} \rightarrow \text{Br}_2 + \text{O}_2$	$2.8 \times 10^{-14} e^{(860/T)}$	1
(R13)	$\text{BrNO}_3 \rightarrow \text{BrO} + \text{NO}_2$	$2.8 \times 10^{13} e^{-(12360/T)}$	2
(R14)	$\text{BrO} + h\nu \rightarrow \text{Br} + \text{O}$	0.05	3
(R15)	$\text{Br}_2 + h\nu \rightarrow 2\text{Br}$	0.0315	3
(R16)	$\text{IBr} + h\nu \rightarrow \text{Br} + \text{I}$	0.067	3
(R17)	$\text{BrCl} + h\nu \rightarrow \text{Br} + \text{Cl}$	9.8×10^{-3}	3
(R18)	$\text{BrNO}_2 + h\nu \rightarrow \text{Br} + \text{NO}_2$	5.8×10^{-3}	3
(R19)	$\text{BrNO}_3 + h\nu \rightarrow \text{BrO} + \text{NO}_2$ ($\Phi = 0.71$) $\rightarrow \text{Br} + \text{NO}_3$ ($\Phi = 0.29$)	1.4×10^{-3}	3
(R20)	$\text{HOBr} + h\nu \rightarrow \text{Br} + \text{OH}$	1.8×10^{-3}	3
(R21)	$\text{CH}_2\text{IBr} + h\nu \rightarrow \text{CH}_2 + \text{Br} + \text{I}$	3.8×10^{-4}	3
(R22)	Uptake coefficient of HOBr	0.05	4
(R23)	Uptake coefficient of HBr	0.03	5
(R2)	Uptake coefficient of BrNO_3	0.02	6

^a Units: unimolecular reactions, s^{-1} ; photolysis rate constants, s^{-1} ; bimolecular reactions, $\text{cm}^3 \text{ molecule}^{-1} \text{ s}^{-1}$; termolecular reactions, $\text{cm}^6 \text{ molecule}^{-2} \text{ s}^{-1}$, calculated using the formalism of Sander et al. (2003a), where $k = ((k_o[M]/(1+k_o[M]/k_\infty)) \times F_c^n)$, $F_c = 0.6$ and $n = (1 + (\log_{10}(k_o[M]/k_\infty))^2)^{-1}$. ^b Remarks: 1, Sander et al. (2003a); 2, from Orlando and Tyndall (1996), applicable for atmospheric pressure; 3, absorption cross-sections taken from Atkinson et al. (2000); 4, from Fickert et al. (1999); Adams et al. (2002); 5, from Schweitzer et al. (1998); 6, from latest IUPAC dataset 2005, estimated from Deiber et al. (2004).

3.6 Modelling the diurnal behaviour of BrO

We now describe a model of bromine chemistry, containing the gas-phase reactions, photochemistry, and heterogeneous uptake processes listed in Table 1. The photolysis rates were calculated off-line using a two-stream radiation scheme. The model is solved using a variable step-size fourth-order Runge-Kutta integrator (Press et al., 1986). All bromine-containing species and O_3 are allowed to vary. The mixing ratios of the following species are held constant at values typical of clean MBL conditions: $[\text{NO}_2] = 30 \text{ ppt}$; $[\text{NO}] = 5 \text{ ppt}$ and 0 ppt at day- and nighttime, respectively; $[\text{DMS}] = 100 \text{ ppt}$; $[\text{CH}_2\text{IBr}] = 0.1 \text{ ppt}$. The mixing ratios of OH and HO_2 are constrained in the model to follow the diurnal profiles of

these radicals measured during NAMBLEX, with noon maxima of 0.1 and 5 ppt, respectively (Bloss et al., 2005). The model also includes the reactions of atomic Br with HCHO and CH_3CHO , using the mixing ratios for these species measured during NAMBLEX (Still et al., 2005; Lewis et al., 2005).

The heterogeneous reaction of HOBr with sea salt and subsequent liberation of Br_2 and BrCl to the gas phase has been observed to occur rapidly (Abbatt and Waschewsky, 1998; Fickert et al., 1999; Adams et al., 2002). These experiments were conducted on surfaces with a Cl^-/Br^- ratio of ~ 660 . Considering the aqueous phase reaction rates and equilibrium constants for Reactions (4)–(6) (Liu and Margerum, 2001; Finlayson-Pitts, 2003), a simple calculation shows that

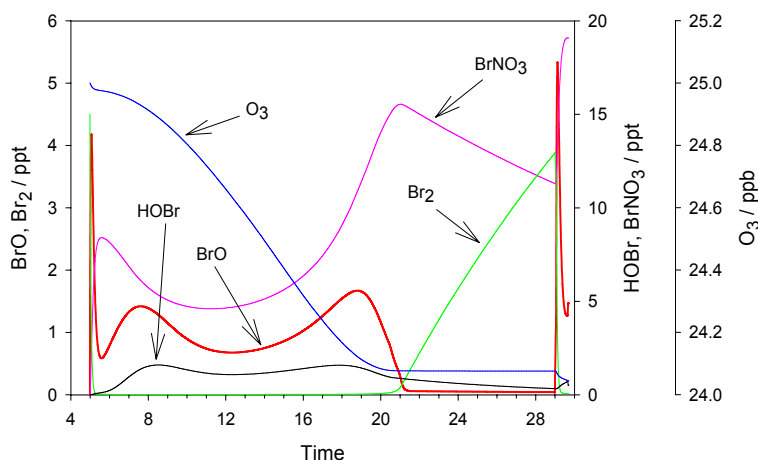
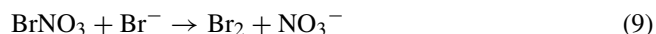
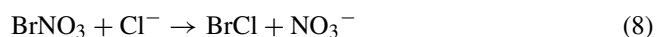


Fig. 13. Model simulation of the diurnal profiles of the main inorganic bromine species and O_3 , for low NO_x conditions in the MBL.

it would take a few minutes for HOBr, once taken up on a sea-salt aerosol surface, to be released as Br_2 and, to a lesser extent $BrCl$, depending upon the Br^- content and acidity of the aerosol (Fickert et al., 1999). Hence, the rate-limiting step of this heterogeneous process will be the uptake of HOBr on the aerosol surface. In the model runs shown here we consider the uptake of HOBr to generate 75% Br_2 and 25% $BrCl$.

Likewise, aqueous phase reactions involving $BrNO_3$ could also lead to the release of Br_2 and $BrCl$ via hydrolysis or reaction with Cl^- and Br^- (Sander et al., 1999):



Reaction of $BrNO_3$ on aerosol surfaces via (8) and (9) can proceed without aerosol acidity, and hence allow halogen activation on alkaline aerosols (Sander et al., 1999). Figure 13 shows the result of a model simulation for clean marine conditions, where the sea-salt surface area is set to $10^{-7} \text{ cm}^2 \text{ cm}^{-3}$ (von Glasow et al., 2002). The model is initialised with Br_2 and $BrCl$ mixing ratios of 4.5 and 1.5 ppt, respectively. A rapid pulse of BrO up to 4.5 ppt is generated as soon as photolysis starts. In order to match the observed pulse of BrO (Fig. 11) the rate of post-sunrise Br atom production required is $\sim 8 \times 10^3 \text{ molecule cm}^{-3} \text{ s}^{-1}$. As Br_2 and $BrCl$ are photolysed and their mixing ratio rapidly decreases, BrO reaches a minimum followed by a slow recovery due to the recycling of HOBr and $BrNO_3$ through sea-salt aerosol. At midday the radical shows a decrease as a result of the diurnal maximum of HOBr, HCHO, CH_3CHO , whereas it increases towards the late afternoon. BrO then disappears as photolysis ceases after sunset. In general, mixing ratios of HCHO and $CH_3CHO > 0.15 \text{ ppb}$ are required in the

model to produce the observed minimum at midday. A similar diurnal behaviour has been predicted in previous studies (Sander et al., 1999; von Glasow et al., 2002). The modelled BrO time-profile in Fig. 13 is comparable to that observed (Fig. 11), with midday/afternoon mixing ratios around 1.5–2.5 ppt. Note that this model does not incorporate BrO mixing within the boundary layer.

After sunset, large amounts of $BrNO_3$ build up as photolysis ceases, and this becomes the major bromine species. In this model run $BrNO_3$ has a loss rate due to uptake on aerosols of $\sim 1 \times 10^{-5} \text{ s}^{-1}$ if $\gamma = 0.02$ (note that the uptake of $BrNO_3$ on deliquesced sea salt aerosols does not appear to have been measured). The daytime average photolysis rate of $BrNO_3$ is $\sim 8.5 \times 10^{-4} \text{ s}^{-1}$, so this will probably be the dominant loss process, competing with thermal decomposition which has a measured rate of $9 \times 10^{-6} \text{ s}^{-1}$ at 290 K (Orlando and Tyndall, 1996). The $BrNO_3$ time-profile in Fig. 13 exhibits two distinct peaks: after the sunrise BrO pulse, and in the early evening when photolysis slows down. The $BrNO_3$ minimum around noon is caused by photolysis, which is sharply peaked to noon because the molecule absorbs almost entirely in the near-UV. After sunset the remaining $BrNO_3$ is slowly taken up on aerosols, and this is most likely the major route to the overnight build-up of gas-phase Br_2 .

HOBr follows the diurnal cycle of HO_2 , with a maximum at midday. HOBr removal during daytime is dominated by photodissociation, as J_{HOBr} is about 40 times greater than heterogeneous loss (which produces Br_2 and $BrCl$). In the present study $\gamma(HOBr) = 0.05$ is used, in accord with a lower limit of $\gamma > 10^{-2}$ measured on aqueous salt solutions (Fickert et al., 1999; Adams et al., 2002). Note that Abbatt and Waschewsky (1998) reported $\gamma > 0.2$ for deliquescent NaCl aerosols within an acidity pH range 0.3–7. The uptake of HOBr and production of gas-phase bromine-containing decreases with decreasing aerosol acidity (Fickert et al., 1999). Here we assume a scenario of freshly generated sea-salt

aerosols with $\text{pH}=8$, the same as ocean water (von Glasow et al., 2002, and references therein). It must be noted that the progressive acidification of aerosols by uptake of species such as HNO_3 , H_2SO_4 and SO_2 is not treated in the model. Considering an average volume concentration of aerosol (diameter= $0.3\text{--}47\ \mu\text{m}$) measured during NAMBLEX of $400\ \mu\text{m}^3\ \text{cm}^{-3}$ (Coe et al., 2005) and a Br^- content in sea salt of $8\times 10^{-3}\ \text{mol l}^{-1}$, we calculate that 22% of Br^- ions would be depleted from the aerosol in one day, giving rise to a gas-phase bromine concentration of $\sim 4\times 10^8\ \text{cm}^{-3}$.

After sunset, the main sink for HOBr is heterogeneous uptake, contributing to the nighttime production of gas-phase bromine atom precursors: Fig. 13 shows the Br_2 build up once photolysis ceases leading to a maximum before sunrise, which will be responsible of the second post-dawn BrO pulse. Note that O_3 is depleted through the day at a rate of approximately $0.06\ \text{ppb h}^{-1}$, mainly through the cycle involving $\text{BrO}+\text{HO}_2$. Of course, this is a zero-dimensional model and does not include mixing with O_3 -rich air from aloft.

Sensitivity studies were then carried out to assess the likely range of $\gamma(\text{BrNO}_3)$ compatible with the observed BrO. The model was now initialised with 10^{-2} ppt of gas-phase Br_2 and BrCl . With $\gamma(\text{BrNO}_3)=0.02$, the halogen recycling through sea-salt aerosol needs four days to release enough photolabile bromine to account for a post-sunrise BrO pulse of 4 ppt. In contrast, for $\gamma(\text{BrNO}_3)$ values of 0.1 and 0.5, the simulation time required is 3 and 2 days, respectively. That is, a higher $\gamma(\text{BrNO}_3)$ reduces the gas-phase BrNO_3 concentration and accelerates the loss of Br^- and Cl^- from aerosols. Further model developments involving aqueous-phase chemistry are the subject of ongoing work.

4 Conclusions

The techniques of long-path DOAS and zenith sky spectroscopy have been employed to acquire a comprehensive set of measurements of I_2 , IO, OIO, BrO and NO_3 in a coastal mid-latitude location. The time series of the different species over a month of observations are summarised in this paper. The observed daytime mixing ratios of the halogen oxides affect a number of atmospheric processes such as ozone depletion, DMS oxidation, formation of new ultrafine aerosol particle, and regulation of the HO_2/OH and NO_2/NO ratios. Model simulations show that the reaction between NO_3 and I_2 probably accounts for the significant nighttime levels of iodine oxides found at Mace Head. The observed pulses of BrO at sunrise, and subsequent diurnal behaviour of the radical, are explained using a model that incorporates initial mixing ratios of photolyzable bromine (in the form of Br_2 and BrCl), and processing of the major daytime bromine reservoirs, BrNO_3 and HOBr, through sea-salt aerosol. However, the NAMBLEX data-set on BrO is quite small and more field observations are needed in order to establish the diurnal behaviour of this radical. Finally, the combination of boundary

layer and vertical profile measurements of NO_3 indicates that this radical often exists at higher concentration in the upper MBL and lower free troposphere, probably reflecting the efficient removal of NO_3 by DMS close to the ocean surface.

Acknowledgements. This work was supported by the Natural Environment Research Council of the UK. The authors wish to thank D. Heard (University of Leeds) for leading the NAMBLEX campaign and B. Allan for helpful discussions.

Edited by: P. Monks

References

- Abbatt, J. P. D. and Waschewsky, G. C. G.: Heterogeneous interactions of HOBr, HNO_3 , O_3 and NO_2 with deliquescent NaCl aerosols at room temperature, *J. Phys. Chem. A*, 102, 3719–3725, 1998.
- Adams, J. W., Holmes, N. S., and Crowley, J. N.: Uptake and reaction of HOBr on frozen and dry NaCl/NaBr surfaces between 253 and 233 K, *Atmos. Chem. Phys.*, 2, 79–91, 2002.
- Alicke, B., Hebestreit, K., Stutz, J., and Platt, U.: Iodine oxide in the marine boundary layer, *Nature*, 397, 572–573, 1999.
- Aliwell, S. R. and Jones, R. L.: Measurement of atmospheric NO_3 2. Diurnal variation of stratospheric NO_3 at midlatitude, *Geophys. Res. Lett.*, 23, 2589–2592, 1996.
- Allan, B. J. and Plane, J. M. C.: A study of the recombination of IO and NO_2 and the stability of INO_3 : implications for the atmospheric chemistry of iodine, *J. Phys. Chem. A*, 106, 8634–8641, 2002b.
- Allan, B. J., Carslaw, N., Coe, H., Burgess, R. A., and Plane, J. M. C.: Observations of the nitrate radical in the marine boundary layer, *J. Atmos. Chem.*, 33, 129–154, 1999.
- Allan, B. J., McFiggans, G., Plane, J. M. C., and Coe, H.: Observations of iodine monoxide in the remote marine boundary layer, *J. Geophys. Res.-Atmos*, 105, 14 363–14 369, 2000a.
- Allan, B. J., McFiggans, G., Plane, J. M. C., and McFadyen, G. G.: The nitrate radical in the remote marine boundary layer, *J. Geophys. Res.-Atmos*, 105, 24 191–24 204, 2000b.
- Allan, B. J., Plane, J. M. C., and McFiggans, G.: Observations of OIO in the remote marine boundary layer, *Geophys. Res. Lett.*, 28, 1945–1948, 2001.
- Allan, B. J., Plane, J. M. C., Coe, H., and Shillito, J. A.: Observations of NO_3 concentration profiles in the troposphere, *J. Geophys. Res.-Atmos*, 107, 4588, doi:10.1029/2002JD002 112, 2002a.
- Ashworth, S. H., Allan, B. J., and Plane, J. M. C.: High resolution spectroscopy of the OIO radical: Implications for the ozone-depleting potential of iodine, *Geophys. Res. Lett.*, 29, 1456, doi:10.1029/2001GL013 851, 2002.
- Atkinson, R., Baulch, D. L., Cox, R. A., Crowley, J. N., R. F. Hampson, J., Hynes, R. G., Jenkin, M. E., Kerr, J. A., Rossi, M. J., and Troe, J.: Summary of evaluated kinetic and photochemical data for atmospheric chemistry, IUPAC, *J. Phys. Chem. Ref. Data*, 29, <http://www.iupac-kinetic.ch.cam.ac.uk/>, 2000.
- Barrie, L. A., Bottenheim, J. W., Schnell, R. C., Crutzen, P. J., and Rasmussen, R. A.: Ozone destruction and photochemical reactions at polar sunrise in the lower Arctic atmosphere, *Nature*, 334, 138–141, 1988.

- Behnke, W., Scheer, V., and Zetzsch, C.: Production of BrNO₂, Br₂ and ClNO₂ from the reaction between sea spray aerosol and N₂O₅, *J. Aero. Sci.*, 25, S277–S278, 1994.
- Behnke, W., George, C., Scheer, V., and Zetzsch, C.: Production and decay of ClNO₂ from the reaction of gaseous N₂O₅ with NaCl solution: bulk and aerosol experiments, *J. Geophys. Res.-Atmos.*, 102, 3795–3804, 1997.
- Bloss, W. J., Lee, J. D., Johnson, G. P., Sommariva, R., Heard, D. E., Saiz-Lopez, A., Plane, J. M. C., McFiggans, G., Coe, H., Flynn, M., Williams, P., Rickard, A. R., and Fleming, Z.: Impact of halogen monoxide chemistry upon boundary layer OH and HO₂ concentrations at a coastal site, *Geophys. Res. Lett.*, 32, L06814, doi:10.1029/2004GL022084, 2005.
- Brown, S. S., Stark, H., Ryerson, T. B., Williams, E. J., Nicks, D. K., Trainer, M., Fehsenfeld, F. C., and Ravishankara, A. R.: Nitrogen oxides in the nocturnal boundary layer: Simultaneous in situ measurements of NO₃, N₂O₅, NO₂, NO, O₃, *J. Geophys. Res.-Atmos.*, 108, 4299, doi:10.1029/2002JD002917, 2003.
- Brown, S. S., Dibb, J. E., Stark, H., Aldener, M., Vozella, M., Whitlow, S., Williams, E. J., Lerner, B. M., Jakoubek, R., Middlebrook, A. M., DeGouw, J. A., Warneke, C., Goldan, P. D., Kuster, W. C., Angevine, W. M., Sueper, D. T., Quinn, P. K., Bates, T. S., Meagher, J. F., Fehsenfeld, F. C., and Ravishankara, A. R.: Nighttime removal of NO_x in the summer marine boundary layer, *Geophys. Res. Lett.*, 31, L07108, doi:10.1029/2004GL019412, 2004.
- Butkovskaya, N. I. and LeBras, G.: Mechanism of the NO₃ + DMS reaction by discharge flow mass-spectrometry, *J. Phys. Chem. A*, 98, 2582–2591, 1994.
- Carpenter, L. J., Sturges, W. T., Penkett, S. A., Liss, P. S., Alicke, B., Hebestreit, K., and Platt, U.: Short-lived alkyl iodides and bromides at Mace Head, Ireland: Links to biogenic sources and halogen oxide production, *J. Geophys. Res.-Atmos.*, 104, 1679–1689, 1999.
- Chambers, R. M., Heard, A. C., and Wayne, R. P.: Inorganic gas-phase reactions of the nitrate radical - I₂+NO₃ and I+NO₃, *J. Phys. Chem. A*, 96, 3321–3331, 1992.
- Coe, H., Allan, B. J., and Plane, J. M. C.: Retrieval of vertical profiles of NO₃ from zenith sky measurements using an optimal estimation method, *J. Geophys. Res.-Atmos.*, 107, 4587, doi:10.1029/2002JD002111, 2002.
- Coe, H., Allan, J. D., Alfarra, M. R., Bower, K. N., Flynn, M. J., McFiggans, G. B., Topping, D. O., Williams, P. I., O'Dowd, C. D., Dall'Osto, M., Beddows, D. C. S., and Harrison, R. M.: Chemical and physical characteristics of aerosol particles at a remote coastal location, Mace Head, Ireland, during NAMBLEX, *Atmos. Chem. Phys. Discuss.*, 5, 11 643–11 678, 2005.
- Davis, D. J., Crawford, J., Liu, S., McKeen, S., Bandy, A., Thornton, D., Rowland, F., and Blake, D.: Potential impact of iodine on tropospheric levels of Ozone and other critical oxidants, *J. Geophys. Res.-Atmos.*, 101, 1996.
- Deiber, G., George, C., Calve, S. L., Schweitzer, F., and Mirabel, P.: Uptake study of ClNO₂ and BrNO₂ by halide containing droplets, *Atmos. Chem. Phys.*, 4, 2004.
- Farman, J. C., Gardiner, B. G., and Shanklin, J. D.: Large losses of total ozone in Antarctica reveal seasonal ClO_x/NO_x interaction, *Nature*, 315, 1985.
- Fickert, S., Adams, J. W., and Crowley, J. N.: Activation of Br₂ and BrCl via uptake of HOBr onto aqueous salt solutions, *J. Geophys. Res.-Atmos.*, 104, 1999.
- Finlayson-Pitts, B. J.: The tropospheric chemistry of sea salt: a molecular-level view of the chemistry of NaCl and NaBr, *Chem. Rev.*, 103, 2003.
- Finlayson-Pitts, B. J., Livingston, F. E., and Berko, H. N.: Ozone destruction and bromine photochemistry at ground-level in the Arctic spring, *Nature*, 343, 1990.
- Frenzel, A., Scheer, V., Sikorski, R., George, C., Behnke, W., and Zetzsch, C.: Heterogeneous interconversion reactions of BrNO₂, ClNO₂, Br₂ and Cl₂, *J. Phys. Chem. A*, 102, 1329–1337, 1998.
- Garland, J. A. and Curtis, H.: Emission of iodine from the sea surface in the presence of ozone, *J. Geophys. Res.-Atmos.*, 86, 3183–3186, 1981.
- Harwood, M. H., Burkholder, J. B., Hunter, M., Fox, R. W., and Ravishankara, A. R.: Absorption cross sections and self-reaction kinetics of the IO radical, *J. Phys. Chem. A*, 101, 853–863, 1997.
- Hausmann, M. and Platt, U.: Spectroscopic measurement of bromine oxide and ozone in the high Arctic during Polar Sunrise Experiment 1992, *J. Geophys. Res.-Atmos.*, 99, 25 399–25 413, 1994.
- Heintz, F., Platt, U., Flentje, H., and Dubois, R.: Long-term observation of nitrate radicals at the Tor station, Kap Arkona (Rugen), *J. Geophys. Res.-Atmos.*, 101, 22 891–22 910, 1996.
- Hönninger, G. and Platt, U.: Observations of BrO and its vertical distribution during surface ozone depletion at Alert, *Atmos. Environ.*, 36, 2481–2489, 2002.
- Holmes, N. S., Adams, J. W., and Crowley, J. N.: Uptake and reaction of HOI and IONO₂ on frozen and dry NaCl/NaBr surfaces and H₂SO₄, *Phys. Chem. Chem. Phys.*, 3, 1679–1687, 2001.
- Ingham, T., Cameron, M., and Crowley, J. N.: Photodissociation of IO(355 nm) and OIO (532 nm): Quantum yields for O(³P) and I(²P₁) production, *J. Phys. Chem. A*, 104, 8001–8010, 2000.
- Jenkin, M. E., Cox, R. A., and Candeland, D. E.: Photochemical aspects of tropospheric iodine behavior, *J. Atmos. Chem.*, 2, 359–375, 1985.
- Joseph, D. M., Ashworth, S. H., and Plane, J. M. C.: The absorption cross-section and photochemistry of OIO, *J. Photochem. Photobiol. A-Chemistry*, 176, 68–77, 2005.
- Kpper, F. C., Schweigert, N., Gall, E. A., Legendre, J. M., Vilter, H., and Kloareg, B.: Iodine uptake in Laminariales involves extracellular, haloperoxidase-mediated oxidation of iodide, *Planta*, 207, 163–171, 1998.
- Leser, H., Hönninger, G., and Platt, U.: MAX-DOAS measurements of BrO and NO₂ in the marine boundary layer, *Geophys. Res. Lett.*, 30, doi:10.1029/2002GL015811, 2003.
- Lewis, A. C., Hopkins, J. R., Carpenter, L. J., Stanton, J., Read, K. A., and Pilling, M. J.: Sources and sinks of acetone, methanol, and acetaldehyde in north Atlantic air, *Atmos. Chem. Phys.*, 5, 1963–1974, 2005.
- Liu, Q. and Margerum, D. W.: Equilibrium and kinetics of bromine chloride hydrolysis, *Environ. Sci. Tech.*, 35, 1127–1133, 2001.
- McConnell, J. C., Henderson, G. S., Barrie, L., Bottenheim, J., Niki, H., Langford, C. H., and Templeton, E. M. J.: Photochemical bromine production implicated in Arctic boundary-layer ozone depletion, *Nature*, 355, 150–152, 1992.
- McFiggans, G., Plane, J. M. C., Allan, B. J., Carpenter, L. J., Coe, H., and O'Dowd, C.: A modeling study of iodine chemistry in the marine boundary layer, *J. Geophys. Res.-Atmos.*, 105, 14 371–14 385, 2000.

- McFiggans, G., Coe, H., Burgess, R., Allan, J., Cubison, M., Alfarra, M. R., Saunders, R., Saiz-Lopez, A., Plane, J. M. C., Wevill, D. J., Carpenter, L. J., Rickard, A. R., and Monks, P. S.: Direct evidence for coastal iodine particles from *Laminaria* macroalgae – linkage to emissions of molecular iodine, *Atmos. Chem. Phys.*, 4, 701–713, 2004.
- Misra, A. and Marshall, P.: Computational investigations of iodine oxides, *J. Phys. Chem. A*, 102, 9056–9060, 1998.
- Molina, M. J. and Rowland, F. S.: Stratospheric sink for chlorofluoromethanes – chlorine atom-catalysed destruction of ozone, *Nature*, 249, 810–812, 1974.
- O'Dowd, C. D., Jimenez, J. L., Bahreini, R., Flagan, R. C., Seinfeld, J. H., Hameri, K., Pirjola, L., Kulmala, M., Jennings, S. G., and Hoffmann, T.: Marine aerosol formation from biogenic iodine emissions, *Nature*, 417, 632–636, 2002.
- Orlando, J. J. and Tyndall, G. S.: Rate coefficients for the thermal decomposition of BrONO_2 and the heat of formation of BrONO_2 , *J. Phys. Chem. A*, 100, 19 398–19 405, 1996.
- Plane, J. M. C. and Saiz-Lopez, A.: UV-visible Differential Optical Absorption Spectroscopy (DOAS), in: *Analytical Techniques for Atmospheric Measurement*, edited by: Heard, D. E., Blackwell Publishing, Oxford, 2006.
- Plane, J. M. C., Joseph, D. M., Allan, B. J., Ashworth, S. H., and Francisco, J. S.: An experimental and theoretical study of the reactions $\text{OIO} + \text{NO}$ and $\text{OIO} + \text{OH}$, *J. Phys. Chem. A*, 110, 93–100, 2006.
- Platt, U., Perner, D., Harris, G. W., Winer, A. M., and Pitts, J. N.: Detection of NO_3 in the polluted troposphere by differential optical absorption, *Geophys. Res. Lett.*, 7, 89–92, 1980.
- Platt, U., LeBras, G., Poulet, G., Burrows, J. P., and Moortgat, G.: Peroxy radicals from night-time reaction of NO_3 with organic compounds, *Nature*, 348, 147–149, 1990.
- Press, W. H., Flannery, B. P., Teukolsky, S. A., and Vetterling, W. T.: *Numerical recipes: The art of scientific computing*, Cambridge University Press, Cambridge, 1986.
- Purvis, R. M., McQuaid, J. B., Lewis, A. C., Hopkins, J. R., and Simmonds, P.: Horizontal and vertical profiles of ozone, carbon monoxide, non-methane hydrocarbons and dimethyl sulphide near the Mace Head observatory, Ireland, *Atmos. Chem. Phys. Discuss.*, 5, 12 505–12 530, 2005.
- Rodgers, C. D.: Retrieval of atmospheric temperature and composition from remote measurements of thermal-radiation, *Rev. Geophys.*, 14, 609–624, 1976.
- Rodgers, C. D.: Characterization and error analysis of profiles retrieved from remote sounding measurements, *J. Geophys. Res.-Atmos.*, 95, 5587–5595, 1990.
- Saiz-Lopez, A. and Plane, J. M. C.: Novel iodine chemistry in the marine boundary layer, *Geophys. Res. Lett.*, 31, 2004.
- Saiz-Lopez, A., Plane, J. M. C., and Shillito, J. A.: Bromine oxide in the mid-latitude marine boundary layer, *Geophys. Res. Lett.*, 31, 2004a.
- Saiz-Lopez, A., Saunders, R. W., Joseph, M., and Plane, J. M. C.: Absolute absorption cross-section and photolysis rate of I_2 , *Atmos. Chem. Phys.*, 4, 2004b.
- Saiz-Lopez, A., Plane, J. M. C., Williams, P. I., McFiggans, G., Ball, S. M., Bitter, M., Hongwei, C., and Hoffmann, T.: Modelling molecular iodine emissions in a coastal marine environment: the link to new particle formation, *Atmos. Chem. Phys.*, 6, 883–895, 2006.
- Sander, R., Rudich, Y., von Glasow, R., and Crutzen, P. J.: The role of BrNO_3 in marine tropospheric chemistry: A model study, *Geophys. Res. Lett.*, 26, 1999.
- Sander, R., Keene, W. C., Pszenny, A. A. P., Arimoto, R., Ayers, G. P., Baboukas, E., Caaney, J. M., Crutzen, P. J., Duce, R. A., Hönninger, G., Huebert, B. J., Maenhaut, W., Mihalopoulos, N., Turekian, V. C., and Dingenen, R. V.: Inorganic bromine in the marine boundary layer: a critical review, *Atmos. Chem. Phys.*, 3, 1301–1336, 2003.
- Sander, S. P., Friedl, R. R., Golden, D. M., Kurylo, M. J., Huie, R. E., Orkin, V. L., Moortgat, G. K., Ravishankara, A. R., Kolb, C. E., Molina, M., and Finlayson-Pitts, B. J.: Chemical kinetics and photochemical data for use in stratospheric modeling: Evaluation 14, Tech. rep., Jet Propulsion Laboratory, Pasadena, California, USA, <http://jpldataeval.jpl.nasa.gov/>, 2003a.
- Schweitzer, F., Mirabel, P., and George, C.: Multiphase chemistry of N_2O_5 , ClONO_2 , BrNO_2 , *J. Phys. Chem. A*, 102, 3942–3952, 1998.
- Smith, J. P. and Solomon, S.: Atmospheric NO_3 . 3. Sunrise disappearance and the stratospheric profile, *J. Geophys. Res.-Atmos.*, 95, 13 819–13 827, 1990.
- Smith, J. P., Solomon, S., Sanders, R. W., Miller, H. L., Perliski, L. M., Keys, J. G., and Schmeltekopf, A. L.: Atmospheric NO_3 . 4. Vertical profiles at middle and polar latitudes at sunrise, *J. Geophys. Res.-Atmos.*, 98, 8983–8989, 1993.
- Still, T. J., Al-Haider, S., Seakins, P. W., Sommariva, R., Stanton, J. C., Mills, G., and Penkett, S. A.: Ambient formaldehyde measurements made at a remote marine boundary layer site during the NAMBLEX campaign - a comparison of data from chromatographic and modified Hantzsch techniques, *Atmos. Chem. Phys. Discuss.*, 5, 12 531–12 567, 2005.
- Thompson, A. M.: The effect of clouds on photolysis rates and ozone formation in the unpolluted troposphere, *J. Geophys. Res.-Atmos.*, 89, 1341–1349, 1984.
- Toumi, R.: BrO as a sink for dimethylsulphide in the marine atmosphere, *Geophys. Res. Lett.*, 21, 117–120, 1994.
- Truesdale, V. W., Luther, G. W., and Canosa-Mas, C.: Molecular iodine reduction in seawater – an improved rate equation considering organic compounds, *Mar. Chem.*, 48, 143–150, 1995.
- Vogt, R., Crutzen, P. J., and Sander, R.: A mechanism for halogen release from sea-salt aerosol in the remote marine boundary layer, *Nature*, 383, 327–330, 1996.
- Vogt, R., Sander, R., von Glasow, R., and Crutzen, P. J.: Iodine chemistry and its role in halogen activation and ozone loss in the marine boundary layer: A model study, *J. Atmos. Chem.*, 32, 375–395, 1999.
- von Glasow, R. and Crutzen, P. J.: Model study of multiphase DMS oxidation with a focus on halogens, *Atmos. Chem. Phys.*, 4, 589–608, 2004.
- von Glasow, R., Sander, R., Bott, A., and Crutzen, P. J.: Modelling halogen chemistry in the marine boundary layer 1. Cloud-free MBL, *J. Geophys. Res.-Atmos.*, 107, 4341, doi:10/1029/2001JD000 942, 2002.
- Vrekoussis, M., Kanakidou, M., Mihalopoulos, N., Crutzen, P. J., Lelieveld, J., Perner, D., Berresheim, H., and Baboukas, E.: Role of the NO_3 radicals in oxidation processes in the eastern Mediterranean troposphere during the MINOS campaign, *Atmos. Chem. Phys.*, 4, 169–182, 2004.

- Wagman, D. D., Evans, W. H., Parker, V. B., Schumm, R. H., Halow, I., Bailey, S. M., Churney, K. L., and Nuttall, R. L.: The NBS tables of chemical thermodynamic properties; Selected values for inorganic and C₁ and C₂ organic substances in SI units, *J. Phys. Chem. Ref. Data*, 11, Suppl. 2, 1982.
- Wahner, A., Ravishankara, A. R., Sander, S. P., and Friedl, R. R.: Absorption cross-section of BrO between 312 and 385 nm at 298 and 223 K, *Chem. Phys. Lett.*, 152, 507–512, 1988.
- Wofsy, S. C., McElroy, M. B., and Yung, Y. L.: The chemistry of atmospheric bromine, *Geophys. Res. Lett.*, 2, 215–218, 1975.
- Yokelson, R. J., Burkholder, J. B., Fox, R. W., Talukdar, R. K., and Ravishankara, A. R.: Temperature-Dependence of the NO₃ absorption spectrum, *J. Phys. Chem. A*, 98, 13 144–13 150, 1994.